Eco Cities 2025, 6(1), 2976.
https://doi.org/10.54517/ec2976

Article

Spatio-temporal analysis of urban heat island dynamics in urban centers landscape of southwest Ethiopia

Tesfaye Dessu Geleta[1,*], Diriba Korecha Dadi[2]

[1] Ethiopian Meteorological Institute, Addis Ababa 1090, Ethiopia
[2] Famine Early Warning Systems Network, Addis Ababa 17483, Ethiopia
*** Corresponding author:** Tesfaye Dessu Geleta, tesfayegyana@gmail.com

CITATION

Geleta TD, Dadi DK. Spatio-temporal analysis of urban heat island dynamics in urban centers landscape of southwest Ethiopia. Eco Cities. 2025; 6(1): 2976. https://doi.org/10.54517/ec2976

ARTICLE INFO

Received: 8 October 2024
Accepted: 22 January 2025
Available online: 18 February 2025

Abstract: Climate change is becoming a global threat to human well-being and the sustainability of the planet Earth. The central cores of urban centers are significantly observed warmer than their surrounding outskirts or rural areas, which is identified as the urban heat island (UHI) effect fueled by massive Land Use Land Cover (LULC) change. The main research aim was to examine the Spatio-temporal variation of UHI dynamics based on the land surface temperature (LST), Normalized Difference Vegetation Index (NDVI) and built-up density in the urban centers (Jimma, Bedelle, Bonga, and Sokorru) landscape using techniques of remote sensing. In this study, Landsat thematic mapper (TM) for 1987 and Landsat Operational Imagery (OLI) for 2018 in the extraction of LST were used for examining UHI. Also, LULC, NDVI and built-up density of the urban centers were analyzed. The results of the study showed that the urban core had greater LST and UHI values, due to an increase of built-up density and a decline of green space. The result of LST mean value range rose from 20.1 ℃ (Bonga) to 23.3 ℃ (Sokorru) in 1987 and 22.67 ℃ (Bedelle) to 24.74 ℃ (Bonga), and 24.72 ℃ (Sokorru) in 2018, while the maximum observed LST value range from 28.97 ℃ (Jimma) in 1987 to 32.61 ℃ (Bonga) in 2018. The maximum range of UHI mean value was from 11.23 ℃ (1987) to 14.04 ℃ (2018), while the maximum observed UHI value ranged from 19.63 ℃ in 1987 to 23.32 ℃ in 2018 over Jimma city. The computed correlation at 5% significance results showed LULC change has a significant association with surface air temperature (r = 0.621, Sig. (2-tailed) = 0.031) accompanied by UHI impacts. We recommended urban authorities, policymakers, and urban planners should consider the effects of LST and UHI in urban planning to realize climate-smart urban centers of tomorrow in urban centers of southwest Ethiopia.

Keywords: urban heat island; land surface temperature; land use; urbanization; NDVI; and built-up density

1. Introduction

Most studies define the term “urbanization” as an increase in the population proportion living in cities and the physical expansion of previously existing urban centers [1]. According to the reports of world urbanization prospect 2018, which predicted that 68% of the world population would reside in the urban areas by the year 2050 [2]. Africa has a low level of urbanization with 37.1% compared to other developed ones like North America (79%) and Europe (72.7%) as reported [1]. While the less urbanized country Ethiopia from Africa is currently only 20% of the population living in urban areas, urbanization is increasing at a rate of 4.4% [2,3].

The most frequent occurrence that raises a city’s surface temperature in comparison to its periphery is known as the “urban heat island (UHI)” [4]. Most

scholars reported that a higher LST in urban centers than in the nearby fringe suburban or rural areas is an urban heat island [5–7]. This phenomenon is triggered by an environmental effect of urbanization and industrialization turning the natural landscapes of urban areas into impervious or impermeable surfaces [8]. Urbanization alters natural into built impervious surfaces, imposing a significant impact on the city's thermal environment [4,9]. There are more artificial surfaces in urban areas than natural or green ones. Once the heat is retained by these man-made surfaces, the land surface temperature (LST) rises and moves upward into the atmosphere and downward into the subsurface layers, heating the surface, the subsurface, and the atmosphere together to create an urban heat island [10]. Observations have shown that the temperatures of urban centers can be up to 12 ℃ higher than neighboring outskirts [11].

Anthropogenic heat emissions are also higher in cities. The surface energy balance at the surface and the layer of boundary structure in and around cities' local UHI circulation systems are altered by these variations in radiation, warm air, and vibrant features [12]. When the rural and urban areas are subjected to the same climate, some of the greatest reported canopy layer-UHI (CL-UHI) are recorded in the summer under clear skies, low wind, and 2–3 h after sunset [12,13]. Some patterns do, however, exist [14] for a variety of reasons: (1) averaging over longer periods with different synoptic conditions within one season or longer; (2) rural and urban areas are not exposed to the same regional climate (i.e., combined effects—not just urban processes); and (3) in some regions, the role of anthropogenic heat flux emissions during winter may be significant.

Increased urban temperatures typically have negative local, regional, and global effects on the economy, health and ecology. These consequences increased the need for air conditioning, increased pollution, altered urban thermal conditions, and caused a rise in the frequency of heat-related illnesses due to persistently high temperatures, which is thermal pollution brought by human activity triggering local microclimate change [15]. The previous study confirmed that local microclimate change is exacerbated by LULC change [16,17]. The occurrence of UHI in urban centers affects the resident's comfortability and their health [18–21]. An increasing trend in UHI impacts the well-being and health of people which contributes to the rising rates of energy consumption, neurological system disorders (such as sleeplessness, irritability, sadness, and memory loss), heart attacks, hyperthermia, diseases of the digestive system, and even violent episodes of high death rates in urban centers [22]. However, the spatio-temporal formation of UHIs phenomena is associated with high intensity of LST caused by the dynamics of LULC [23]. While understanding urban climates and providing integrated urban services is aided by an analysis of urban center UHI [24].

Urban centers are more conducive to the establishment of UHIs due to a number of factors, including the loss of flora, the high-water impermeability of structures, and the materials used to pave roadways. Furthermore, the characteristics of construction materials combined with the daily activities of the occupants could lead to reduced wind speeds, air pollution, and anthropogenic heat [25]. The built-up and vegetation index showed a substantial link in the study on the ecological assessment of UHI occurrences in Chicago [26]. An empirical verification,

evaluation, and forecasting conducted over Cumilla showed Bangladesh's seasonal urban thermal field variance index (UTFVI) and UHI [27]. The origins, impacts, and remedies for UHI effects were also expounded [28]. Another study examined the effects of terrain and building or construction materials in a thorough analysis of the UHI intensity effects in East African metropolitan cities [29].

The previously conducted research in Ethiopia by [30], carried out investigations on the factors that cause UHI in Hawassa city, which tried to mention the role of geological processes basically resulting from hot rocks near the city. Also, another study carried out by [31], which assessed the UHI dynamics over Jimma city due to LULC change. Another study conducted over the four fast-growing cities in Ethiopia (Adama, Addis Ababa, Hawassa and Bahir Dar) that associates green space dynamics with LST intensity [32]. Also, another study in Mekelle city pointed out UHI variation and its impact over the city for 30 years by using the remote sensing techniques [33].

Extensive and measurable data are needed to comprehend what was/is happening and predict the scenario in the near future because urbanization spurred the UHI occurrence and repercussions on human well-being. The harshness of the urban climate, however, received less attention in the past and little research has been done to determine how urbanization alters surface temperature and UHI as well as its impact on the local microclimate of urban centers of southwest Ethiopia. Therefore, the main purpose of this research was to examine the spatiotemporal variation and trends of UHI, LST, NDVI, and built-up density nexus using remote sensing techniques on four urban centers of southwest Ethiopia (Jimma, Bedelle, Bonga and Sokorru) from 1987–2018. These urban centers have social and economic importance for the region and are growing rapidly, with Jimma as the central hub and the others nearly located at 100 km horizontal ground distance, which was selected purposively. The area is considered the wettest part of the country, due to unplanned urban development without consideration of urban planning, the urban centers environmental challenges and climate change footprints impacts becoming evident as reported by previous studies. These study findings will alert the urban actors to consider the climate change issues for sustainable urban development planning to reverse the problems ahead. As research gaps, the four urban centers less studied using GIS and remote sensing-based satellite images or data with particular urban landscapes setting. The previous research focuses on major cities more than the middle emerging ones and the lack of up-to-date land use land cover. Satellite & GIS data at the town/city level limits the study, which needs intensive data to carry out in-depth analysis, making insufficient studies.

Furthermore, this study will play a pivotal role in providing baseline information for urban actors (urban planners, urban authorities, policy makers, residents and researchers) that curbs scant literature in this regard. This complements the finding of adaptation and mitigation climate actions that enable sustainable, climate-smart urban centers of the future and motivate researchers to conduct future research on urban problems. In addition, these study findings can be relevant to other cities with comparable socioeconomic and demographic features.

2. Materials and methods

2.1. Study area description

This study was conducted in the southwest Ethiopia's urban area, which lies between 7°22′ N to 8°45′ N and 36°23′ E to 37°40′ E representing a grid box of 1° × 1°. The urban centers located in the Oromia Regional State are Jimma, Bedelle, and Sokorru, while Bonga is in the Southern Nations Nationalities and Peoples (SNNP), as depicted in **Figure 1**. The altitude ranges from 600 to over 2000 m while the altitude of Jimma City ranges from 1720 m above sea level (m.a.s.l) at Airport (Kitto) to the maximum 2010 m.a.s.l of Jiren at Abba Jifar Palace (Masara). Whereas, Bonga (1779), Bedelle (2011), and Sokorru (1928) m.a.s.l. elevation (**Figure 1**) [16,34,35]. According to the City's revised master plan 2019, the total land area of Jimma City is about 10,200 hectares, while that of Bonga is 8846, Bedelle is 2878, and Sokorru is 300 hectares.

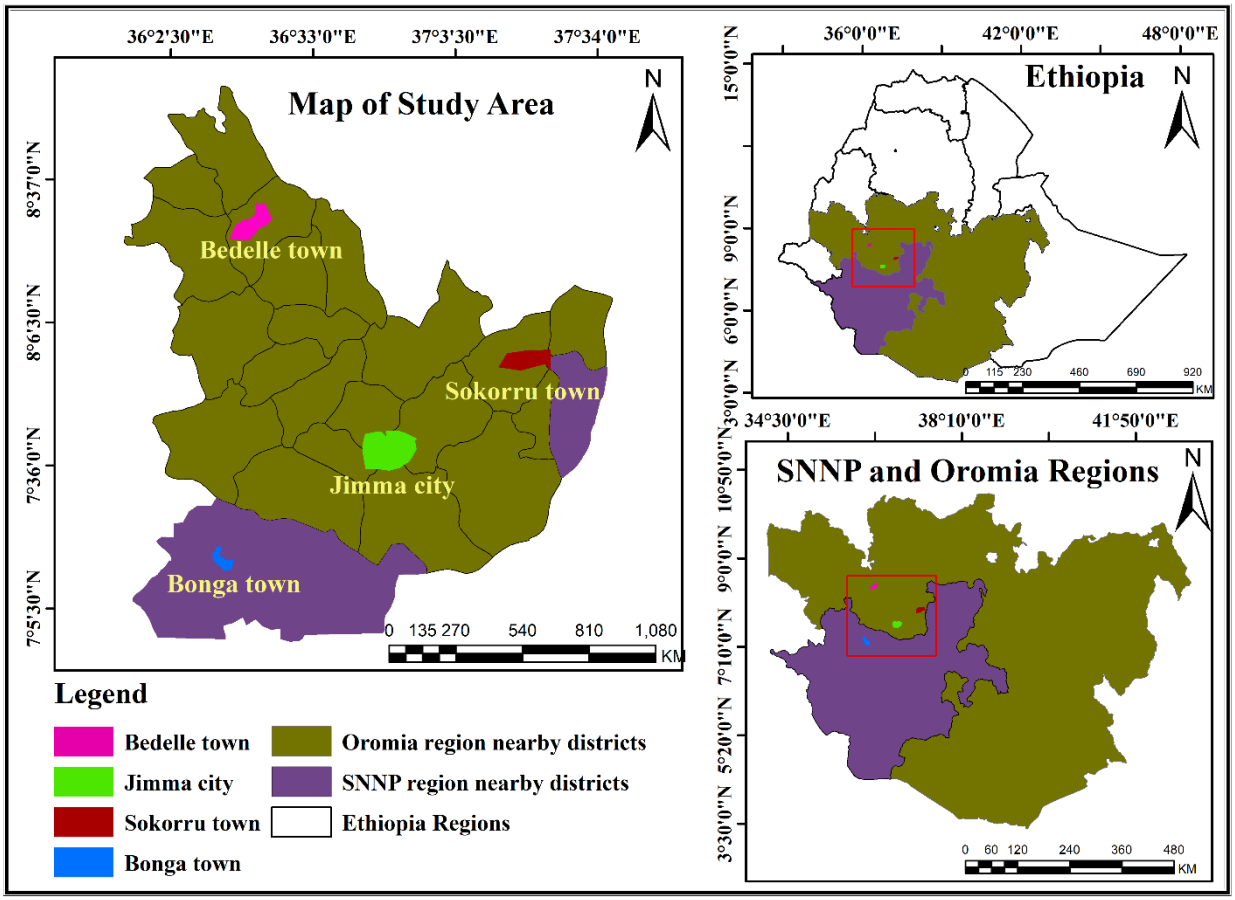

Figure 1. The study area location map.

The total populations living in study urban centers are in Jimma City (265,000), Bonga 44,046 (by 2024); Bedelle (40,500) and that of Sokorru (25,617) in the year 2024 [36,37].

Climatically, the annual temperature mean was between 19–20 ℃ and the annual mean rainfall ranges from 1700–2000 mm (**Figure 2**). The highest monthly mean temperature was experienced at 21.5 ℃ on Sokorru in March and the lowest

17.7 ℃ on Bedelle in July from 1990–2020 (**Figure 2**). The area is experienced with a mono-modal rainfall type, with the main rainy season—from the middle of March to October—and the small rainy season—February to April (**Figure 2**). Comparatively, Bedelle receives the highest annual rainfall total, followed by Jimma, Bonga, and the lowest in Sokorru, with 1931, 1844, 1809, and 1379 mm, respectively, from observed meteorological data computed from 1990–2020 (**Figure 2**). Whereas the driest months are November, December, and January, the highest mean temperature is observed in March and April due to the proximity of the location near the tropics (**Figure 2**). The southwest of Ethiopia is the uppermost rainfall-receiving and the wettest corridor in the country, as documented by many studies [38,39].

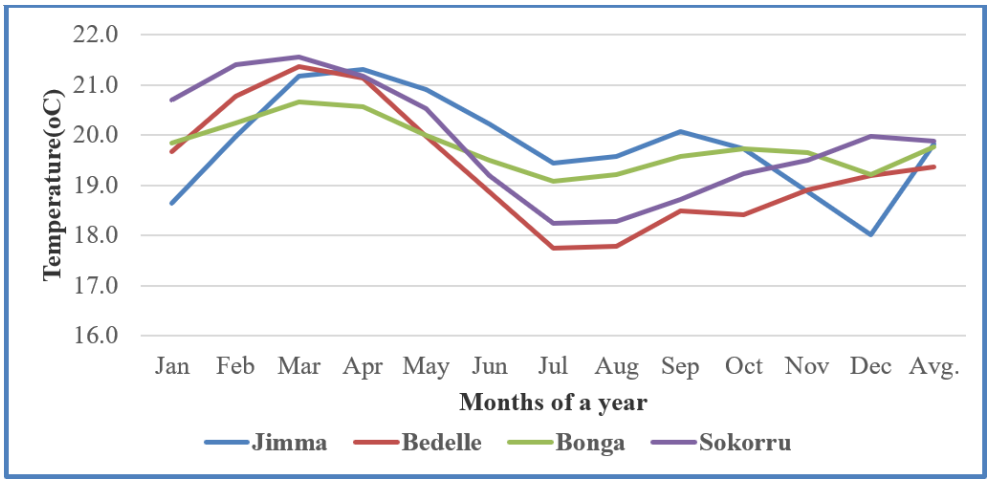

(a)

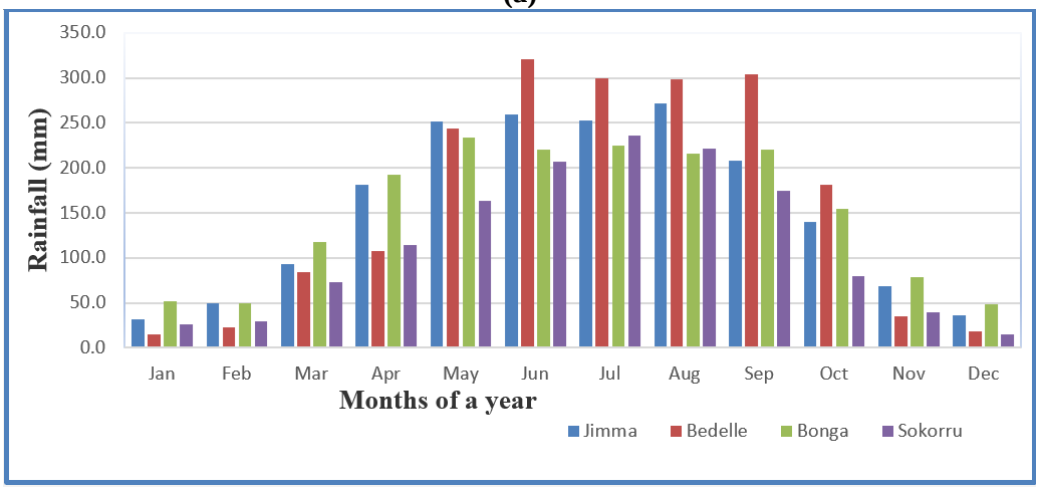

(b)

Figure 2. Computed study urban centers' **(a)** monthly mean temperature; **(b)** monthly rainfall totals from 1990–2020.

The significant business activity is contributed by local urban-rural exchanges. Commerce is the basic economic action with small manufacturing enterprises. Also, the livelihood of households depends on surrounding natural resources and urban agriculture as well as labor employments in different enterprises like small-scale cottage industries. Concerning the infrastructure development, the towns are interconnected by a highway asphalt road that runs from Addis Ababa to Sokorru-Jimma-Bonga via the Mizzen route and from Jimma-Agaro-Bedelle, which runs to

the Metu-Gambella or Nekemte route. Comparatively, Jimma city has a well-developed infrastructure, and Sokorru is less developed with respect to others. Bonga and Bedelle have gotten administration special attention as well.

2.2. Data sources

The Landsat Thematic Mappers (TMs) of 1987 and Landsat Operational Land Imager (OLI) of 2018 images of the dry period were downloaded from the USGS website via (http://earthexplorer.usgs.gov) at a resolution of 30 m, which was cloud-free (**Table 1**). The months were selected based on the availability of the finest cloud-free/minimum satellite imagery for thermal LST assessment and spectral index analysis. The image analyses were conducted using ERDAS software version of 2015, and change analysis was conducted using supervised classification maximum likelihood algorithms following change detection procedures. For climate data sources, long years of data series for air temperature (1987–2018) were collected from the Ethiopian Meteorological Institute (EMI). Linear regression analysis and the Mann-Kendall test were conducted as well using relevant analytical tools.

Table 1. Data source description.

S/No.	Urban center	Source	Acquisition Year		Path/Row	Resolution (m)	Software used
			1987 Landsat (TM)	2018 Landsat (OLI)			
1	Jimma	USGS	22/11/1987	27/11/2018	169/055	30	ERDAS 2015, Arc GIS10.5 for LU/LCC, LST, UHI, NDVI and, built-up map analysis, SPSS version 23
2	Sokorru	USGS	24/12/1987	24/12/2018	170/054	30	
3	Bedelle	USGS	15/11/1987	20/11/2018	170/055	30	
4	Bonga	USGS	15/11/1987	20/11/2018	169/055	30	

2.3. Land surface temperature analysis

There are several well-developed algorithms used for the retrieval of LSTs from Landsat TM and OLI/TIRAS data, including mono-window algorithms [40] and split-window algorithms [41]. Alternatively, image-based single-band split-window algorithms were used to retrieve LST values from Landsat images thermal bands because the method is less sensitive to uncertainties in the optical properties of the atmosphere, which was analytically efficient [42]. It uses the brightness temperature of band 10 of thermal infrared (TIR), the mean, and the difference in land surface emissivity to estimate the surface temperature [43].

Before retrieval of the LST, a quadratic model was utilized to change the digital number of Landsat thermal bands because every object emits thermal electromagnetic energy as its temperature is above absolute zero (k). Based on this principle, the signal received by the thermal sensors (TM and OLI/TIRS) was converted to the sensor radiance ($L\lambda$). The spectral radiance was calculated using the following equation [44]. Moreover, LST retrieval was conducted using Landsat 8 OLI can be analyzed using the following procedures:

2.3.1. Procedure 1: Conversion of digital number into radiance

In radiometric calibration, pixel values, which were represented by Q in remote sensing and unprocessed image data, were thereby changed into absolute radiance

values. Digital numbers are manually changed to at-sensor radiances, then to brightness temperature [45]. The TM and ETM+ DN values range between 0 and 255 (for Landsat 5 and 7). For Landsat 8 OLI using Equation (1):

$$L\lambda = ML \times Qcal + AL - Oi \quad (1)$$

$$L\lambda = 0.0003342 \times Band10 + 0.10000 - 0.29,$$

where:

Lλ—Top of Atmosphere (TOA) spectral radiance (Wm^{-2} sr^{-1} μm^{-1}).

ML-Band-specific multiplicative rescaling factor from the metadata (RADIANCE_MULT_BAND_x, where x is the band number).

AL—Band-specific additive rescaling factor from the metadata (RADIANCE_ADD_BAND_x, where x is the band number).

Qcal—Quantized and calibrated standard product pixel values (DN).

Oi—Correction value for band 10, i.e., 0.29.

2.3.2. Procedure 2: Conversion of radiance to brightness temperature

The TM Band 6 imagery could be transformed from spectral radiance (as described above) to a more physically useful variable. The effective temperature at the satellite of the observed Earth-atmosphere system was computed under uniform emissivity using the constants from pre-launch calibration. The conversion formula is using Equation (2):

$$T = \frac{K2}{\ln\left(\frac{K1}{L\lambda} + 1\right)} \quad (2)$$

T—Effective at-satellite temperature in Kelvin.

K2—Calibration constant two.

K1—Calibration constant one.

L—Spectral radiance in watts/(meter squared × ster × μm).

For Landsat TM and ETM+, the thermal band calibration constants are: Constant 1-K1watts/(meter squared × ster × μm) is 607.76 for Landsat 5. Constant 2-K2 in kelvin is 1260.56 Landsat 5 (Landsat Handbook). The process of analyzing LST values follows the conversion of thermal infrared Digital Numbers (DNs) of Bands 10 to radiance Top of Atmosphere (TOA) and at-satellite brightness temperature. Plank's function was used to examine the effective at-sensor brightness temperature (TB), also known as black body temperature, using the spectral radiance.

In this study, the LST was calculated using the mono-window algorithm [46]. To comprehend the amount of temperature recorded, brightness temperature was approximated [47,48]. In order to comprehend the mean land surface emissivity and subsequently estimate the LST, the brightness temperatures of Landsat 8 (band 10) were estimated [49]. Equation (5) was used to calculate the split-window algorithm's conversion of radiance to temperature [50] was calculated using Equation (5). Using pre-launch calibration constants for the Landsat 8 OLI sensor, spectral radiance readings for band 10 were translated to radiant surface temperature under the presumption of uniform emissivity. The raw digital numbers of the thermal bands are

converted to Top of Atmosphere (TOA) brightness temperatures, which are the effective temperatures seen by the satellite under the assumption of emissivity, after spectral radiance is converted to radiance [51] using Planck's equation. Top of Atmosphere Spectral Radiance was calculated using Equation (3).

$$BT = \frac{K2}{ln\left(\frac{K1}{L\lambda} + 1\right)} \tag{3}$$

where;

BT—effective at-sensor brightness temperature (K);

*K*2—calibration constant 2 (K);

*K*1—calibration constant 1 (W/(m^2 × sr × μm));

Lλ—spectral radiance at the sensor's aperture (W/(m^2 × sr × μm)); and,

ln—a natural logarithm.

2.3.3. Procedure 3: Land surface emissivity estimation

To calculate the LSE, it is crucial to identify the inherent features of the earth's surface and the thermal radiance energy change throughout calculating LST [50,52]. According to [52], the emissivity value for this study was calculated using the following Equation (4).

$$\varepsilon = 0.004 \times PV + 0.986 \tag{4}$$

While *PV* is the vegetation proportion computed using the proceeding formula;

$$\mathrm{PV} = \left[\frac{\mathrm{NDVImax} - \mathrm{NDVImin}}{\mathrm{NDVImax} - \mathrm{NDVImin}}\right]^2 \tag{5}$$

The computed radiant surface temperatures were corrected for emissivity as used by [53] using Equation (6):

$$LST = \frac{TB}{1(\lambda TB/P)In\varepsilon} \tag{6}$$

where;

LST—land surface temperature (in Kelvin), *TB*—radiant surface temperature (in Kelvin).

λ—the wavelength of emitted radiance (11.5 μm), *ρ*—$h \times c \div \sigma$ (1.438 × 10^{-2} mK).

h—Planck's constant (6.26 × 10^{-34} J·s), *c*: is the velocity of light (2.998 × 10^8 m/s).

σ—Stefan Boltzmann's constant (1.38 × 10^{-23} J·K^{-1}), and *ε*—land surface emissivity.

To convert land surface temperature value from the kelvin unit to degrees Celsius.

$$\mathrm{LST\ (0celsius)} = \mathrm{LST\ (Kelvin)} - 273.15 \tag{7}$$

2.4. Validation of LST retrieved

The validation process was done by using the LST value being extracted using zonal statistics from Landsat LST. Finally, land surface temperature values

from Landsat 5 TM and Landsat 8 OLI were verified using meteorological temperature data. Therefore, meteorological temperature data was used from the station located in the study urban centers.

2.5. Analysis of UHI dynamics in urban centers landscape

To identify the UHI crucial areas determined by the distribution of LST and the amount of vegetation cover, LST was measured using an equation developed by [53,54]. Also, to compare UHI variation for different times, normalization methods of LST were performed following [55] and [27] by using where urban heat was characterized using the following Equation (8) formula:

$$UHI = Ts - Tm/Sd \quad (8)$$

Ts—Land surface temperature.
Tm—The mean of LST.
Sd—The standard deviation of LST.

2.6. Normalized difference vegetation index (NDVI) extraction

The green spaces of urban spatial distribution in the study urban centers were extracted and computed based on NDVI value. The NDVI value generally ranges between −1 and +1. The −1 value implies the absence of vegetation, while +1 values the presence of dense vegetation. While NDVI values are feasible for the computation of change detection analysis, with NDVI low value (0.1 and below) showing barren areas of sand, rock, or snow [56]. The NDVI value is further categorized as no-vegetation (for the value < 0), unhealthy vegetation (0.02–0.03), and bush and grasses represent moderate values (0.2 to 0.3), while a high NDVI value shows dense vegetation ranging from 0.6 to 0.8 [57]. NDVI was acquired from spectral measurements of reflectance in the visible (Red) and near-infrared regions (NIR) in the ArcGIS environment. OLI's visible, near-infrared, and short-wave infrared bands were used to compute the NDVI of the four urban centers, each using the formula:

$$\text{NDVI} = \frac{NIR - R}{NIR + R} \quad (9)$$

where: *NIR*—pixel digital number (DN) of TM Band 4 and Band 5 (for Landsat 7 and 8, respectively) as well as *R*—DN of TM Band 3 and Band 4 (for Landsat7 and 8 respectively) [58].

LST, which is the radiative temperature over the surface of land influenced by albedo, soil moisture, and the vegetation covers, was measured by remote sensing, whereas air temperature is measured 1–2 m above the ground using instrumentation techniques. The intricate interactions of turbulent heat transfers are generated by surrounding hot surfaces, resulting in the temperature of the air close to the surface [58]. Generally, for LST, UHI, NDVI and built-up data analysis for each of the four urban centers, the software used were ArcGIS 10.5 for analyzing and visualizing spatial data, ERDAS 2015 for image classification and accuracy assessment, Google Earth Pro and GPS for LULC accuracy assessment, and SPSS V23 for regression and correlation analysis.

3. Results

3.1. Spatio-temporal analyzed result of LST over urban centers

To create a distribution of thermal patterns for each of the four urban centers on the map, LST distribution was categorized into the proper ranges and color-coded. The findings showed that study urban centers have different LST values due to differences in the LULC classes. The highest computed minimum and maximum land surface temperature increase in 1987 and 2018 was observed in Bonga, which ranges from 4–5 ℃, followed by Jimma with 2.6–2.8 ℃, Sokorru 1.3–1.6 ℃, and the least in Bedelle 0.5–1.2 ℃ (**Table 2**).

The highest LST values were observed in open areas (vacant spaces) and built-up areas with a drastic increase of impervious structure surfaces during the past thirty years as a result of urban growth in urban areas. The detail summary value of LST for each urban center's minimum versus maximum LST for the 1987 and 2018 years is depicted in **Table 2**. The varied trends of LST are connected to the thermal properties of different types of LULC classes. The thermal signature of each kind of land cover was obtained by superimposing a land surface temperature image with a land use and land cover map from 1987 and 2018 to better understand how urban growth affects land surface temperatures (**Figure 3**, **Table 2**).

The findings of the analyzed LST for the four urban centers revealed that the lowest minimum and the highest maximum LST values rose from 12.7 ℃ (Bonga) and 29 ℃ (Jimma) in the year 1987 to 15.6 ℃ (Jimma) and 23.3 ℃ (Bonga) in the year 2018, respectively (**Figure 3**, **Table 2**).

Table 2. Computed results of LST, UHI and NDVI values of urban centers in 1987 and 2018.

Urban centers	**Landsat TM 1987 LST values (℃)**			**Landsat OLI 2018 LST values (℃)**		
	Minimum	**Maximum**	**Mean**	**Minimum**	**Maximum**	**Mean**
Jimma	12.84	28.97	20.91	15.64	31.64	23.64
Sokorru	18.28	28.26	23.30	19.85	29.59	24.72
Bedelle	16.90	26.90	21.90	17.42	27.92	22.67
Bonga	12.67	27.51	20.10	16.86	32.61	24.74
Urban centers	Landsat TM 1987 UHI values (℃)			Landsat OLI 2018 UHI values (℃)		
	Minimum	Maximum	Mean	Minimum	Maximum	Mean
Jimma	3.62	19.63	11.23	4.76	23.32	14.04
Sokorru	4.44	14.75	10.20	9.02	17.47	13.23
Bedelle	2.24	12.60	7.42	2.42	13.21	7.93
Bonga	2.41	13.34	8.00	3.38	23.31	13.35
Urban centers	Landsat TM 1987 NDVI values			Landsat OLI 2018 NDVI values		
	Minimum	Maximum	Mean	Minimum	Maximum	Mean
Jimma	−0.33	0.73	0.30	−0.06	0.58	0.26
Sokorru	0.08	0.65	0.37	0.07	0.47	0.27
Bedelle	0.04	0.65	0.35	0.06	0.42	0.24
Bonga	0.03	0.69	0.36	0.04	0.61	0.33

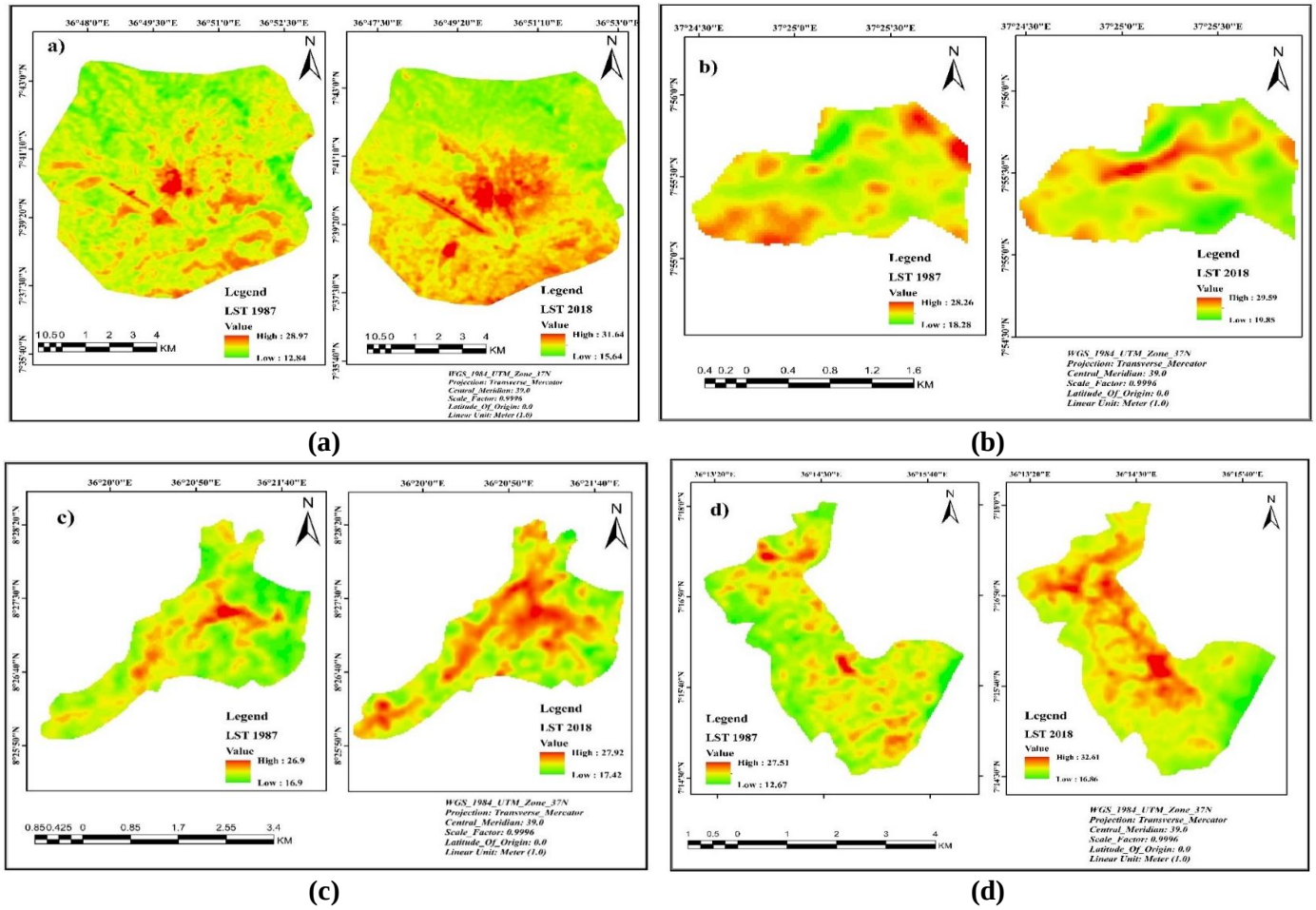

Figure 3. Land surface temperature map of **(a)** Jimma; **(b)** Sokorru; **(c)** Bedelle; **(d)** Bonga in 1987 and 2018.

3.2. Spatial analysis of urban heat island variation in urban centers landscape

The findings revealed that the lowest minimum and the highest maximum UHI rose from 2.2 ℃ (Bedelle) and 19.6 ℃ (Jimma) in the year 1987 to 2.4 ℃ (Bedelle) and 23.3 ℃ (Jimma) in the year 2018, respectively (**Table 2**; **Figure 4**). The primary cause of the change was the substitution of impervious or impermeable surfaces for green space. The highest value of UHI was seen in parts with a high concentration of complex buildings and construction and low vegetation cover (**Table 2**; **Figure 4**).

The analysis of the UHI in the four urban centers revealed that the highest UHI was from 3.6 to 19.6 ℃ in Jimma for the minimum and highest maximum values, respectively, whereas the lowest UHI was observed from 2.2 to 12.6 ℃ in Bedelle for the minimum and maximum values, respectively, in the year of 1987. Also, the computed result revealed that the highest UHI was from 4.8 to 23.3 ℃ in Jimma, respectively for the minimum and maximum values, whereas the lowest UHI was observed from 2.4 to 13.2 ℃ in Bedelle, for minimum and maximum values, respectively, in the year 2018 (**Table 2**; **Figure 4**). The detail summary value of UHI for each urban center's minimum versus maximum in the 1987 and 2018 years is depicted in **Table 2**.

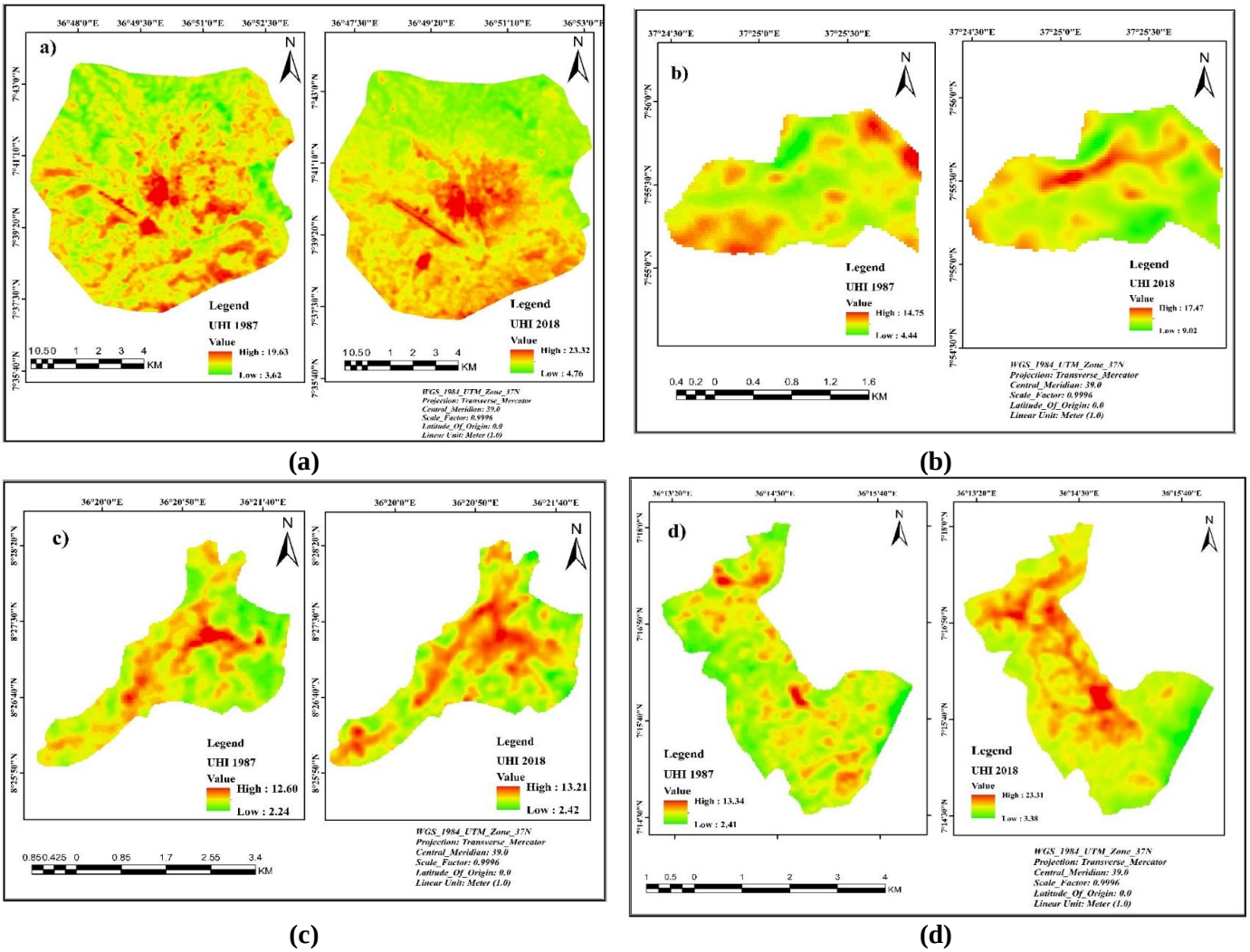

Figure 4. Urban heat island (UHI) map of **(a)** Jimma; **(b)** Sokorru; **(c)** Bedelle; **(d)** Bonga in the year 1987 and 2018.

3.3. Analyzed result of normalized difference of vegetation index (NDVI)

According to the computed results of the NDVI of study urban centers for both the years 1987 and 2018, the greater NDVI value was experienced in the highest vegetation coverage in the study of 4 urban centers and vice versa. The highest NDVI value was observed in the patches of forests, riverbanks, and wetlands, with vegetation in the surrounding peripheries (**Figure 5**). The analysis of NDVI revealed that both the NDVI minimum and maximum values declined from 1987 to 2018 in the recent past 30 years (**Tables 2** and **3**; **Figure 5**). The computed findings revealed that the decline of NDVI value from 1987, which implies the vegetation coverage reduced in the year 2018. The decline of vegetation complements the upsurge or increase of LST and UHI effects in urban centers. Thus, the reduction of vegetation cover results in temperature increase due to reduction in cooling effect, which in turn means NDVI is negatively correlated with LST as well (**Table 3**). The urban centers local communities and administrations have to emphasize the green spaces development in their urban landscape jurisdiction.

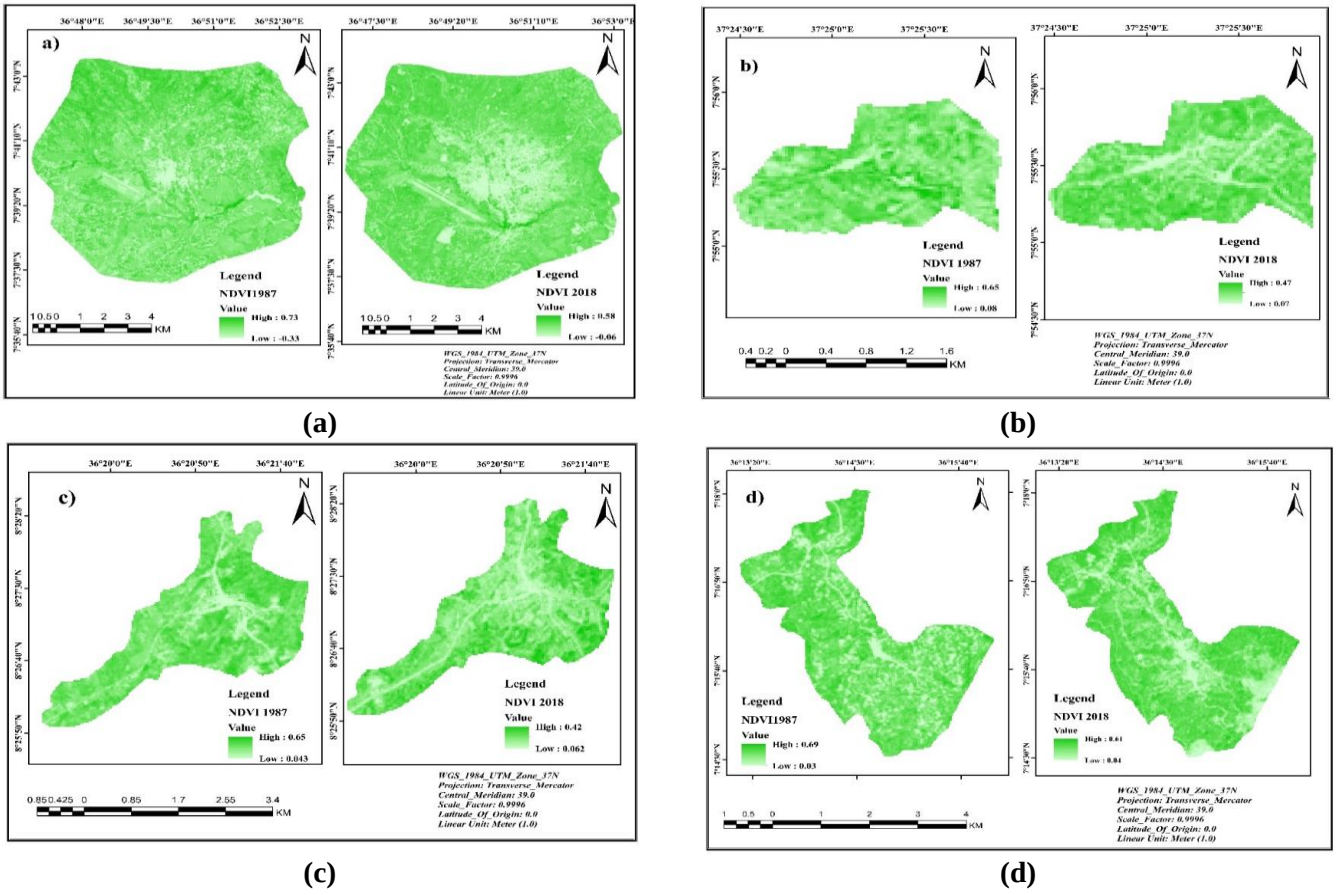

Figure 5. Normalized difference vegetation index map for **(a)** Jimma; **(b)** Sokorru; **(c)** Bedelle; **(d)** Bonga in 1987 and 2018.

Table 3. Computed correlation analysis between vegetation cover change and microclimate changes inducing LST in urban landscapes.

Correlations[a]						
		Rain fall in mm	**TempMax**	**TempMi**	**Tmean in oC**	**LULCC in Ha**
Rain fall in mm	Pearson Correlation	1	−1.000**	−1.000**	−1.000**	0.153
	Sig. (2-tailed)		0.000	0.000	0.000	0.717
	N	8	8	8	8	8
TempMax	Pearson Correlation	−1.000**	1	1.000**	1.000**	−0.153
	Sig. (2-tailed)	0.000		0.000	0.000	0.717
	N	8	8	8	8	8
TempMin	Pearson Correlation	−1.000**	1.000**	1	1.000**	−0.153
	Sig. (2-tailed)	0.000	0.000		0.000	0.717
	N	8	8	8	8	8
Tmean in oC	Pearson Correlation	−1.000**	1.000**	1.000**	1	−0.153
	Sig. (2-tailed)	0.000	0.000	0.000		0.717
	N	8	8	8	8	8
LULCC in Ha	Pearson Correlation	0.153	−0.153	−0.153	−0.153	1
	Sig. (2-tailed)	0.717	0.717	0.717	0.717	
	N	8	8	8	8	8

**. Correlation is significant at the 0.01 level (2-tailed).
[a]. LULC type = vegetation, LULCC- Land Use Land Cover Change.

3.4. Spatio-temporal analysis of built-up dynamics in urban centers landscape

Concerning the built-up density, the 4 urban centers built up significantly increased from the years 1957/58/67, 1987, and 2018 with respect to individual urban land size (**Table 4**; **Figure 6**). Comparatively, the Jimma city built-up area increased from 220 ha (2%) in the past 1957 to 2580 ha (23%) in 2018; in Sokorru the built-up area increased from 20 ha (6%) in 1957 to 116 ha (36%) in 2018; in Bedelle the area of built-up enlarged from 43 ha (5%) in 1958 to 325 ha (38%) in 2018; and in Bonga the increase of built-up area from 54 ha (4%) in 1957 to 297 ha (22%) in 2018 (**Table 4**; **Figure 6**). Although, due to the absence of shortwave infrared in 1957/58/67 and 1987, the NDBI was not generated, rather than the increase of built-up trend density from 1957–2018 was depicted using the table below (**Table 4**; **Figure 6**).

The non-parametric correlation analysis implied that there is a significant relationship between LULCC in Ha with RF and Tmin, which shows that as LULCC in Ha increases, RF and Tmin may increase moderately (r = 0.621, p = 0.031); however, there is no statistical association between LULCC in Ha with other climate variables (**Tables 4** and **5**). Also, the regression analysis in all urban centers shows that the surface temperature increases as urbanization increases during the recent past of 30 years due to built-up increase at the expense of vegetation reduction (**Tables 4–6**). Thus, the higher the vegetation cover depicted, the higher the value of NDVI, which showed a negative association between LST and NDVI.

Table 4. LULC change and type of (ha, %) of a) Jimma, b) Sokorru, c) Bedelle, and d) Bonga from the 1950s to the 2010s.

		Share of LULC from the total area of each urban center						**LULC change in hectare (ha)**		
	LULC Type	**1957/58/67**		**1987**		**2018**		**1957/58/67–1987**	**1987–2018**	**1957–2018**
		ha	**%**	**ha**	**%**	**ha**	**%**	**ha**	**ha**	**ha**
a) Jimma (1957)	Cropland	3036	29	2774	27	2566	22	−262	−208	−470
	Vegetation	4307	41	4644	44	2880	25	337	−1764	−1427
	Wetland	2901	28	2674	26	3438	30	−227	764	537
	Built-up	220	2	372	3	2580	23	152	2208	2360
b) Sokorru (1957)	Cropland	129	41	119	37	82	26	−10	−37	−47
	Vegetation	98	31	83	26	66	21	−15	−17	−32
	Wetland	71	22	67	21	54	17	−4	−13	−17
	Built-up	20	6	49	16	116	36	29	67	96
c) Bedelle (1958)	Cropland	265	31	238	28	189	22	−27	−49	−67
	Vegetation	436	51	352	41	251	29	−84	−101	−185
	Wetland	108	13	106	13	87	10	−2	−19	−21
	Built-up	43	5	156	18	325	38	113	169	282
d) Bonga (1967)	Cropland	463	34	443	32	395	29	−20	−48	−68
	Vegetation	664	49	589	43	548	40	−75	−59	−116
	Wetland	187	14	145	11	128	9	−42	−17	−59
	Built-up	54	4	191	14	297	22	137	106	243

Table 5. Computed correlation analysis between LULCC and microclimate changes in urban landscapes.

Correlations							
			LULCC in Ha	**Rainfall**	**Tmax**	**Tmin**	**Tmean**
Spearman's rho	LULCC in Ha	Correlation Coefficient	1.000	0.621*	−0.355	0.621*	0.266
		Sig. (2-tailed)		0.031	0.258	0.031	0.403
	RF	Correlation Coefficient	0.621*	1.000	−0.500	1.000**	0.500
		Sig. (2-tailed)	0.031		0.098		0.098
	Tmax	Correlation Coefficient	−0.355	−0.500	1.000	−0.500	0.500
		Sig. (2-tailed)	0.258	0.098		0.098	0.098
	Tmin	Correlation Coefficient	0.621*	1.000**	−0.500	1.000	0.500
		Sig. (2-tailed)	0.031		0.098		0.098
	Tmean	Correlation Coefficient	0.266	0.500	0.500	0.500	1.000
		Sig. (2-tailed)	0.403	0.098	0.098	0.098	

*. Correlation is significant at the 0.05 level (2-tailed).
**. Correlation is significant at the 0.01 level (2-tailed), bold stands for correlation and significant values.

The regression analysis and Mann-Kendall test results showed over four urban centers under study the temperature change observed, which was a consequence of urbanization that leads to LULCC. Thus, especially the NDVI is negatively correlated with LST and positively associated with built-up area increase, but the change varies spatio-temporally among urban centers (**Tables 4** and **6**).

Table 6. Linear regression and Mann-Kendall test of temperature results (1967–2018) in urban centers of southwest Ethiopia at a 95% confidence interval.

S/N	**Attribute**	**Jimma**	**Bedelle**	**Bonga**	**Sokorru**
I	Minimum Temperature				
	change of temp (℃/year)	0.028	0.057	−0.002	0.021
	change of temp (℃/decade)	0.28	0.57	−0.02	0.21
	R^2	0.393	0.533	0.000	0.178
	Z-value	2.35	2.34	1.43	2.32
	Sen's slope	0.014	0.027	0.010	0.035
II	Maximum temperature				
	change of temp (℃/year)	0.037	0.013	0.076	0.012
	change of temp (℃/decade)	0.37	0.13	0.76	0.12
	R^2	0.67	0.062	0.66	0.000
	Z-value	2.17	3.28	1.63	2.37
	Sen's slope	0.023	0.160	0.000	0.031
III	Mean temperature 0.032 (℃/year) 0.32 (℃/decade), R^2 = 0.705				

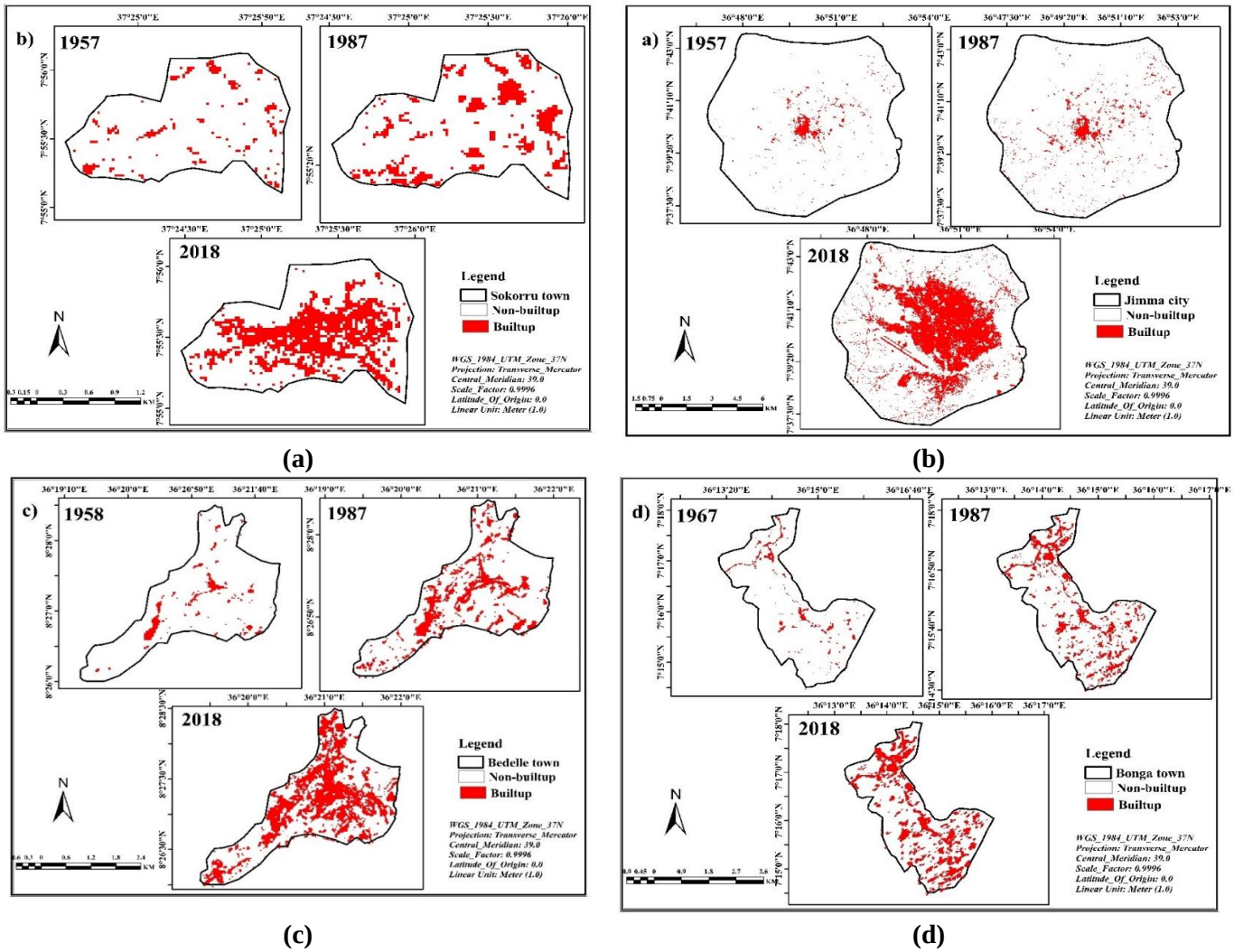

Figure 6. Built-up areas map of **(a)** Jimma; **(b)** Sokorru; **(c)** Bedelle; **(d)** Bonga in 1957/58/67, 1987 and 2018.

4. Discussion

The computed study findings implied that the urban central core of the study towns had greater LST and UHI values, which are associated with the extent of built-up area density and LULC spatial coverage of specific urban centers, which was consistent with the studies of previous works [2] and impervious surface coverage [59,60]. The computed result of LST mean value range rose from 20.1 ℃ (Bonga) to 23.3 ℃ (Sokorru) in 1987 and 22.67 ℃ (Bedelle) to 24.74 ℃ (Bonga) and 24.72 ℃ (Sokorru) in 2018, while the maximum observed LST value ranged from 28.97 ℃ (Jimma) in 1987 to 32.61 ℃ (Bonga) in 2018 (**Table 2**; **Figures 3** and **4**). The findings show that the UHI maximum mean value range was from 11.23 ℃ (1987) to 14.04 ℃ (2018) experienced, while the maximum observed UHI value range was from 19.63 ℃ in 1987 to 23.32 ℃ in 2018 over Jimma city (**Table 2**; **Figures 3** and **4**). The primary cause of the change was the substitution of impervious or impermeable surfaces like wetlands, cropland and green space to other land uses of the urban centers under study. Over Delhi city, similar findings have been recorded [61].

The highest value of UHI is seen in a high concentration of complex buildings and construction areas in the urban core with less coverage of vegetation (**Tables 2** and **3**; **Figures 4–6**). This finding is comparable with other studies conducted in Jimma city [31] and over Mekelle city [33] which assessed UHI dynamics associated with LULC. This finding agreed with the assertion made by [47] that the LST decreases when the NDVI increases and vice versa. Similar studies disclosed that the opposite association between LST and NDVI has been documented [62–66]. The lack of greenery or vegetation coverage in the city is linked to lower NDVI values in the city of Bahir Dar, Ethiopia [47] which complements our study findings. Also, our findings were consistent with a study on the green space-LST nexus in the four fast-growing major cities in Ethiopia [32], which focus on green spaces role in reducing UHI effects of warming and vice versa, where surface temperature and UHI effect were high in the urban core of study urban centers. In addition, changes in LULC fueled by urbanization affect the local microclimate of study urban centers which varies spatially and temporally, as coined in previous works (**Tables 2** and **3**) [16].

The highest built-up density values were noted in the urban center's highest density built-up areas, while the lowest built-up density values are observed in the lowest built-up density areas. High-density vegetation in urban centers results in lower built-up density and vice versa [67,68]. A study that employed GIS data and RS images used RS images that outperformed in classifying local climate zones in LST and UHI analysis conducted in Guagzhou, China [69]. Similarly, this study tried to utilize the mentioned datasets. The other study conducted in the Wuhan urban agglomeration of China concludes that human activity shows a significant positive correlation, while weather and climate have a negative correlation with the LST, highest in winter [70] and LULCC worsened UHI by impacting thermal comfort [71]. Even though the study context varies, our findings of the weather and climate change are triggered or fueled by human activity of urbanization inducing LST and UHI. By lowering perceived temperatures by up to 20% in vegetated and shaded zones, green spaces have been shown to improve bioclimatic comfort [72], which is similar to our findings of UHI high, where less vegetation cover exists in the urban core of urban centers in southwest Ethiopia.

Moreover, the presence of densely built-up areas results in high built-up density values and vice versa. Therefore, urban development has to be adjusted according to the variability of changing climate and endorse effective urban planning consideration of green spaces in adaptation and mitigation actions ahead to enhance the climate-resilient smart urban centers in Southwest Ethiopia in particular and urban areas of Ethiopia in general.

As the limitations of the study, to curb limitations, even if the authors try to download the RS satellite images during the dry season and cloud-free to optimize the accuracy at that time captured when compared with the current emerged technologies with high resolution, there is a limitation. Also, uncertainties due to certain GIS administrative datasets may not promptly represent urban formations, and due to the rapid rate of unplanned urban expansion, local neighborhoods and communities may not be represented by training samples' coverage locations for classification. In addition, associated factors that limit the LST and UHI formation have to be considered due to urban landscape changes by human actions. Further

studies are suggested to use high spatial resolution satellite data with detailed land use by comparing it with ground reality verification and using models that need testing before use, as well as different UHI mitigation and urban cooling strategies that are studied in urban landscapes.

5. Conclusion

The phenomena of urbanization-triggered climate change occurrence calls for the urgent need to identify the variables that affect LST and UHI, which burden urban actors to curb such ruins in urban centers to implement appropriate adaptation and mitigation actions that match the local context to be more resilient and comfort residents. This study examines the UHI dynamics versus LST, NDVI and built-up density over the recent past 30 years from 1987 to 2018 by GIS and remote sensing methods. Also, assessed how UHI dynamics nexuses and major urbanization factors influenced LST intensity due to vegetation coverage deterioration, which affects the potential cooling intensity of urban centers studied. The urban LULC change dynamics reflect substantial increases in built-up coverage, accompanied by decreases in wetlands, urban green areas, and urban agriculture coverage. Besides, UHI intensity spatial coverage is extensive among urban centers, while computed values showed the high temperature was experienced in the epicenter of urban core areas. Whereas, by 2018, high temperatures in the outskirt's suburban areas of each study urban center revealed intensified or aggravated conditions comparatively. The results implied that rapid urbanization/urban expansion in the four study urban centers has contributed to LULC dynamics that triggered UHI effects due to natural vegetation alteration to built-up areas. UHI and LST rise of increased built-up areas and the decrease of green spaces in all urban centers studied from 1987 to 2018. While growing the extent of green space can greatly reduce or mitigate UHI impacts. The computed correlation analysis result revealed that LULC change had an association with the microclimate change of minimum temperature and rainfall in the southwest Ethiopian urban centers.

Generally, the study findings have practical implications to alert urban actors (urban planners and administrations, residents and others) to thereby implement environmentally sound development. Urban centers of developing countries' emerged in an unplanned way, and similarly, studying urban center development was at the cost of urban environments by impacting their local climate. Therefore, we recommend local government authorities should have to devise local strategies that promote a sustainable path of urban development by involving all urban actors. These strategies could include conservation of green areas in landscape planning that mitigate UHI effects, appropriate use of grey or hard infrastructures, and proper implementation of urban plans by employing adaptation and mitigation climate actions in short- and long-term periods. Finally, urban centers become livable and comfortable to their dwellers and become climate-smart, resilient cities of tomorrow in the dynamic challenge of climate change. Future research could have to consider socioeconomic data, high-resolution satellite images like aerial photography, QuickBird, and other recent RS datasets for more detailed information in this regard.

Author contributions: Conceptualization, TDG; design the manuscript, TDG and DKD; investigation, TDG; data compilation and entry, TDG; data analysis and experimental details, TDG; interpretation of results, TDG; editing and write-up of the manuscript, TDG and DKD; supervision, DKD; made valuable comments, DKD. All authors have read and agreed to the published version of the manuscript.

Acknowledgments: The authors would like to acknowledge the following institutions: United States Geological Survey (USGS), Jimma, Bedelle, Bonga and Sokorru City Administration Offices, Ethiopia Geo-Spatial Institute, and West Oromia Meteorological Services Center of Ethiopian Meteorological Institute. We are also grateful to those friends who stand on our side during the experimental analysis of the research work.

Data availability statement: The data supporting the conclusions are presented in this article but the others will be made available based on reasonable request of the authors.

Conflict of interest: The authors declare no conflict of interest.

References

1. Kassahun S, Tiwari A. Urban development in Ethiopia: challenges and policy responses. Available online: https://ssrn.com/abstract=2154776 (accessed on 10 September 2024).
2. Yu Z, Yao Y, Yang G, et al. Strong contribution of rapid urbanization and urban agglomeration development to regional thermal environment dynamics and evolution. Forest Ecology and Management. 2019; 446: 214-225. doi: 10.1016/j.foreco.2019.05.046
3. Ministry of Finance and Economic Development (MoFED). Ethiopia: Building on Progress: A Plan for Accelerated and Sustained Development to End Poverty (PASDEP). Ministry of Finance and Economic Development (MoFED), Addis Ababa. 2006. Available online: https://www.afdb.org/fileadmin/uploads/afdb/Documents/Policy-Documents/Plan_for_Accelerated_and_Sustained_%28PASDEP%29_final_July_2007_Volume_I_3.pdf (accessed on 10 September 2024).
4. Kim SW, Brown RD. Urban heat island (UHI) intensity and magnitude estimations: A systematic literature review. Science of The Total Environment. 2021; 779: 146389. doi: 10.1016/j.scitotenv.2021.146389
5. Doan VQ, Kusaka H, Nguyen TM. Roles of past, present, and future land use and anthropogenic heat release changes on urban heat island effects in Hanoi, Vietnam: Numerical experiments with a regional climate model. Sustainable Cities and Society. 2019; 47: 101479. doi: 10.1016/j.scs.2019.101479
6. Nwakaire CM, Onn CC, Yap SP, et al. Urban heat island studies with emphasis on urban pavements: a review. Sustain Cities Society. 2020; 63:102476. doi: 10.1016/j.scs.2020.102476
7. Wang L, Hou H, Weng J. Ordinary least squares modelling of urban heat island intensity based on landscape composition and configuration: A comparative study among three megacities along the Yangtze River. Sustainable Cities and Society. 2020; 62: 102381. doi: 10.1016/j.scs.2020.102381
8. Matloob A, Sarif MdO, Um JS. Evaluating the inter-relationship between OCO-2 XCO2 and MODIS-LST in an Industrial Belt located at Western Bengaluru City of India. Spatial Information Research. 2021; 29(3): 257-265. doi: 10.1007/s41324-021-00396-4
9. Sadiq Khan M, Ullah S, Sun T, et al. Land-Use/Land-Cover Changes and Its Contribution to Urban Heat Island: A Case Study of Islamabad, Pakistan. Sustainability. 2020; 12(9): 3861. doi: 10.3390/su12093861
10. Coutts AM, Beringer J, Tapper NJ. Impact of Increasing Urban Density on Local Climate: Spatial and Temporal Variations in the Surface Energy Balance in Melbourne, Australia. Journal of Applied Meteorology and Climatology. 2007; 46(4): 477-493. doi: 10.1175/jam2462.1
11. Voogt JA. Urban Heat Island. In: Munn T (editor). Encyclopedia of Global Environmental Change. Wiley, Chichester; 2002. pp. 660-666.

12. Oke TR, Mills G, Christen A, et al. Urban climates. Cambridge: Cambridge University Press; 2017.
13. Oke TR. Canyon geometry and the nocturnal urban heat island: Comparison of scale model and field observations. Journal of Climatology. 1981; 1(3): 237-254. doi: 10.1002/joc.3370010304
14. World Meteorological Organization (WMO). WMO Guidance on the Canopy Layer Urban Heat Island. 2021. doi: 10.5194/ems2021-301, 2021
15. Zhou Z, Xie Q. Impact of Urbanization on Urban Heat Island and Effect Based on TM Imagery in Wuhan China. Environmental Engineering and Management Journal. 2015; 14(3): 647-655. doi: 10.30638/eemj.2015.072
16. Dessu T, Korecha D, Hunde D, et al. Long-Term Land Use Land Cover Change in Urban Centers of Southwest Ethiopia From a Climate Change Perspective. Frontiers in Climate. 2020; 2. doi: 10.3389/fclim.2020.577169
17. Yuvaraj RM. Extents of predictors for land surface temperature using multiple regression model. Scientific World Journal. 2020. doi: 10.1155/2020/3958589
18. Zhang B, Xie G di, Gao J xi, et al. The cooling effect of urban green spaces as a contribution to energy-saving and emission-reduction: A case study in Beijing, China. Building and Environment. 2014; 76: 37-43. doi: 10.1016/j.buildenv.2014.03.003
19. He BJ. Towards the next generation of green building for urban heat island mitigation: Zero UHI impact building. Sustainable Cities and Society. 2019; 50: 101647. doi: 10.1016/j.scs.2019.101647
20. Qiao Z, Liu L, Qin Y, et al. The Impact of Urban Renewal on Land Surface Temperature Changes: A Case Study in the Main City of Guangzhou, China. Remote Sensing. 2020; 12(5): 794. doi: 10.3390/rs12050794
21. Intergovernmental Panel on Climate Change (IPCC). Climate Change 2022—Impacts, Adaptation and Vulnerability: Working Group II Contribution to the Sixth Assessment Report of the Intergovernmental Panel on Climate Change. Cambridge University Press; 2023.
22. Amani-Beni M, Zhang B, Xie GD, et al. Impacts of Urban Green Landscape Patterns on Land Surface Temperature: Evidence from the Adjacent Area of Olympic Forest Park of Beijing, China. Sustainability. 2019; 11(2): 513. doi: 10.3390/su11020513
23. Portela CI, Massi KG, Rodrigues T, et al. Impact of urban and industrial features on land surface temperature: Evidences from satellite thermal indices. Sustainable Cities and Society. 2020; 56: 102100. doi: 10.1016/j.scs.2020.102100
24. Grimmond S, Bouchet V, Molina LT, et al. Integrated urban hydrometeorological, climate and environmental services: Concept, methodology and key messages. Urban Climate. 2020; 33: 100623. doi: 10.1016/j.uclim.2020.100623
25. Wang H, Zhang Y, Tsou J, et al. Surface Urban Heat Island Analysis of Shanghai (China) Based on the Change of Land Use and Land Cover. Sustainability. 2017; 9(9): 1538. doi: 10.3390/su9091538
26. Alfraihat R, Mulugeta G, Gala TS. Ecological evaluation of urban heat island in Chicago city, USA. Journal of Atmospheric Pollution. 2016; 4(1): 23–29. doi: 10.12691/jap-4-1-3
27. Kafy AA, Abdullah-Al-Faisal, Rahman MdS, et al. Prediction of seasonal urban thermal field variance index using machine learning algorithms in Cumilla, Bangladesh. Sustainable Cities and Society. 2021; 64: 102542. doi: 10.1016/j.scs.2020.102542
28. Nuruzzaman Md. Urban Heat Island: Causes, Effects and Mitigation Measures—A Review. International Journal of Environmental Monitoring and Analysis. 2015; 3(2): 67. doi: 10.11648/j.ijema.20150302.15
29. Li X, Stringer LC, Dallimer M. The Spatial and Temporal Characteristics of Urban Heat Island Intensity: Implications for East Africa's Urban Development. Climate. 2021; 9(4): 51. doi: 10.3390/cli9040051
30. Chaka DS, Oda TK. Understanding land surface temperature on rift areas to examine the spatial variation of urban heat island: the case of Hawassa, southern Ethiopia. GeoJournal. 2019; 86(2): 993-1014. doi: 10.1007/s10708-019-10110-5
31. Moisa MB, Merga BB, Gemeda DO. Urban heat island dynamics in response to land use land cover change: a case of Jimma city, southwestern Ethiopia. Theoretical and Applied Climatology. 2022; 149(1-2): 413-423. doi: 10.1007/s00704-022-04055-y
32. Degefu MA, Argaw M, Feyisa GL, et al. Dynamics of green spaces- Land surface temperature intensity nexus in cities of Ethiopia. Heliyon. 2023; 9(2): e13274. doi: 10.1016/j.heliyon.2023.e13274
33. Tesfamariam S, Govindu V, Uncha A. Spatio-temporal analysis of urban heat island (UHI) and its effect on urban ecology: The case of Mekelle city, Northern Ethiopia. Heliyon. 2023; 9(2): e13098. doi: 10.1016/j.heliyon.2023.e13098
34. Jimma City Administration. Spatial Planning and Socioeconomic Assessment of the Master Plan Under the Revision Document. Jimma City Administration. 2019.

35. Ethiopian Meteorological Institute. Delivering world-class weather and climate services to Ethiopia. Available online: http://www.ethiomet.gov.et (accessed on 1 September 2024).
36. Central Statistical Agency (CSA). Population Statistical Abstract. Addis Ababa: Federal Democratic Republic of Ethiopia, Population Census Commission. 2007. Available online: http://www.statsethiopia.gov.et/wp-content/uploads/2019/06/Population-and-Housing-Census-2007-National_Statistical.pdf (accessed on 10 September 2024).
37. Central Statistical Agency (CSA). Population Projections for Ethiopia, Addis Ababa. Addis Ababa: Population Census Commission; 2017. pp. 2007-2037.
38. Kebede G, Bewket W. Variations in rainfall and extreme event indices in the wettest part of Ethiopia. SINET: Ethiopian Journal of Science. 2009; 32(2). doi: 10.4314/sinet.v32i2.68864
39. Korecha D, Sorteberg A. Construction of Homogeneous Rainfall Regimes for Ethiopia. International Journal of Climatology. 2013. Available online: https://malaria.w.uib.no/files/2014/06/DiribaPhD.pdf (accessed on 20 September 2024).
40. Qin Q, Zhang N, Nan P, et al. Geothermal area detection using Landsat ETM+ thermal infrared data and its mechanistic analysis—A case study in Tengchong, China. International Journal of Applied Earth Observation and Geoinformation. 2011; 13(4): 552-559. doi: 10.1016/j.jag.2011.02.005
41. Jiménez-Muñoz JC, Sobrino JA. A generalized single-channel method for retrieving land surface temperature from remote sensing data. Journal of Geophysical Research: Atmospheres. 2003; 108(D22). doi: 10.1029/2003jd003480
42. Lo CP, Quattrochi DA. Land-Use and Land-Cover Change, Urban Heat Island Phenomenon, and Health Implications. Photogrammetric Engineering & Remote Sensing. 2003; 69(9): 1053-1063. doi: 10.14358/pers.69.9.1053
43. Cheng X, Wei B, Chen G, et al. Influence of park size and its surrounding urban landscape patterns on the park cooling effect. Journal of Urban Planning and Development. 2015; 141(3): 4014002. doi: 10.1061/(ASCE)UP.1943-5444.0000256
44. Landsat Project Science Office. Landsat science data user's handbook. Available online: https://www.usgs.gov/landsat-missions/landsat-data-user-handbooks (accessed on 1 September 2024).
45. Wang L, Hou H, Weng J. Ordinary least squares modelling of urban heat island intensity based on landscape composition and configuration: A comparative study among three megacities along the Yangtze River. Sustainable Cities and Society. 2020; 62: 102381. doi: 10.1016/j.scs.2020.102381
46. Ramachandran J, Lalitha R, Sivasubramanian K. Remote Sensing Based Land Surface Temperature Analysis in Diverse Environment of Lalgudi Block. International Journal of Environment and Climate Change. 2019: 142-149. doi: 10.9734/ijecc/2019/v9i330103
47. Balew A, Korme T. Monitoring land surface temperature in Bahir Dar city and its surrounding using Landsat images. The Egyptian Journal of Remote Sensing and Space Science. 2020; 23(3): 371-386. doi: 10.1016/j.ejrs.2020.02.001
48. Guha S, Govil H, Gill N, et al. A long-term seasonal analysis on the relationship between LST and NDBI using Landsat data. Quaternary International. 2021; 575-576: 249-258. doi: 10.1016/j.quaint.2020.06.041
49. Naeem S, Cao C, Qazi W, et al. Studying the Association between Green Space Characteristics and Land Surface Temperature for Sustainable Urban Environments: An Analysis of Beijing and Islamabad. ISPRS International Journal of Geo-Information. 2018; 7(2): 38. doi: 10.3390/ijgi7020038
50. Kumari B, Tayyab M, Shahfahad, et al. Satellite-Driven Land Surface Temperature (LST) Using Landsat 5, 7 (TM/ETM+ SLC) and Landsat 8 (OLI/TIRS) Data and Its Association with Built-Up and Green Cover Over Urban Delhi, India. Remote Sensing in Earth Systems Sciences. 2018; 1(3-4): 63-78. doi: 10.1007/s41976-018-0004-2
51. Chander G, Markham B. Revised landsat-5 tm radiometric calibration procedures and postcalibration dynamic ranges. IEEE Transactions on Geoscience and Remote Sensing. 2003; 41(11): 2674-2677. doi: 10.1109/tgrs.2003.818464
52. Sobrino JA, Jiménez-Muñoz JC, Paolini L. Land surface temperature retrieval from LANDSAT TM 5. Remote Sensing of Environment. 2004; 90(4): 434-440. doi: 10.1016/j.rse.2004.02.003
53. Effat H, Taha L, Mansour K. Change Detection of Land cover and Urban Heat Islands using Multi-Temporal Landsat Images, application in Tanta City, Egypt. Open Journal of Remote Sensing and Positioning. 2014; 1(2): 1-15. doi: 10.15764/rsp.2014.02001
54. Maheng D, Ducton I, Lauwaet D, et al. The Sensitivity of Urban Heat Island to Urban Green Space—A Model-Based Study of City of Colombo, Sri Lanka. Atmosphere. 2019; 10(3): 151. doi: 10.3390/atmos10030151
55. Abutaleb K, Ngie A, Darwish A, et al. Assessment of Urban Heat Island Using Remotely Sensed Imagery over Greater Cairo, Egypt. Advances in Remote Sensing. 2015; 04(01): 35-47. doi: 10.4236/ars.2015.41004

56. Pervaiz S, Shirazi AS, Khan FZ. Tree census of urban green space with special reference to Gora Cemetery of Lahore, Pakistan. International Journal of Biosciences (IJB). 2018; 13(01): 431-439. doi: 10.12692/ijb/13.1.431-439
57. Gandhi GM, Parthiban S, Thummalu N, et al. Ndvi: Vegetation Change Detection Using Remote Sensing and Gis—A Case Study of Vellore District. Procedia Computer Science. 2015; 57: 1199-1210. doi: 10.1016/j.procs.2015.07.415
58. Avdan U, Jovanovska G. Algorithm for Automated Mapping of Land Surface Temperature Using LANDSAT 8 Satellite Data. Journal of Sensors. 2016; 2016: 1-8. doi: 10.1155/2016/1480307
59. Moisa MB, Dejene IN, Merga BB, et al. Impacts of land use/land cover dynamics on land surface temperature using geospatial techniques in Anger River Sub-basin, Western Ethiopia. Environmental Earth Sciences. 2022; 81(3). doi: 10.1007/s12665-022-10221-2
60. Stemn E, Kumi-Boateng B. Modelling of land surface temperature changes as determinant of urban heat island and risk of heat-related conditions in the Wassa West Mining Area of Ghana. Modeling Earth Systems and Environment. 2020; 6(3): 1727-1740. doi: 10.1007/s40808-020-00786-x
61. Mallick J, Kant Y, Bharath BD. Estimation of land surface temperature over Delhi using Landsat-7 ETM+. The Journal of Indian Geophysical Union. 2008; 12(3): 131–140.
62. Huong NTL, Yao S, Fahad S. Assessing household livelihood vulnerability to climate change: The case of Northwest Vietnam. Human and Ecological Risk Assessment: An International Journal. 2018; 25(5): 1157-1175. doi: 10.1080/10807039.2018.1460801
63. Zare M, Drastig K, Zude-Sasse M. Tree Water Status in Apple Orchards Measured by Means of Land Surface Temperature and Vegetation Index (LST–NDVI) Trapezoidal Space Derived from Landsat 8 Satellite Images. Sustainability. 2019; 12(1): 70. doi: 10.3390/su12010070
64. Merga BB, Moisa MB, Negash DA, et al. Land surface temperature variation in response to landuse and land-cover dynamics: a case of Didessa River sub-basin in western Ethiopia. Earth System Science. 2022; 6: 803-815. doi: 10.1007/s41748-022-00303-3
65. Moisa MB, Merga BB, Gemeda DO. Multiple indices-based assessment of agricultural drought: A case study in Gilgel Gibe Sub-basin, Southern Ethiopia. Theoretical and Applied Climatology. 2022; 148(1-2): 455-464. doi: 10.1007/s00704-022-03962-4
66. Wolteji BN, Bedhadha ST, Gebre SL, et al. Multiple Indices Based Agricultural Drought Assessment in the Rift Valley Region of Ethiopia. Environmental Challenges. 2022; 7: 100488. doi: 10.1016/j.envc.2022.100488
67. Alexander C. Normalised difference spectral indices and urban land cover as indicators of land surface temperature (LST). International Journal of Applied Earth Observation and Geoinformation. 2020; 86: 102013. doi: 10.1016/j.jag.2019.102013
68. Sarif MdO, Gupta RD. Modelling of trajectories in urban sprawl types and their dynamics (1988-2018): a case study of Prayagraj City (India). Arabian Journal of Geosciences. 2021; 14(14). doi: 10.1007/s12517-021-07573-7
69. Xu X, Qiu W, Li W, et al. Comparing satellite image and GIS data classified local climate zones to assess urban heat island: A case study of Guangzhou. Frontiers in Environmental Science. 2022; 10. doi: 10.3389/fenvs.2022.1029445
70. Xu C, Huang G, Zhang M. Comparative Analysis of the Seasonal Driving Factors of the Urban Heat Environment Using Machine Learning: Evidence from the Wuhan Urban Agglomeration, China, 2020. Atmosphere. 2024; 15(6): 671. doi: 10.3390/atmos15060671
71. Hu C, Zhang M, Huang G, et al. Tracking the Impact of the Land Cover Change on the Spatial-Temporal Distribution of the Thermal Comfort: Insights from the Qinhuai River Basin, China. Sustainable Cities and Society. 2024; 116. doi.org/10.1016/j.scs.2024.105916
72. Zhang M, Yiğit İ, Adigüzel F, et al. Impact of Urban Surfaces on Microclimatic Conditions and Thermal Comfort in Burdur, Türkiye. Atmosphere. 2024; 15(11): 1375. doi: 10.3390/atmos15111375